Protein Science (1997), *6*:2504–2511. Cambridge University Press. Printed in the USA.

Crystal structures of a marginally active thymidylate synthase mutant, Arg 126 → Glu

PAVEL STROP,[1] LIMING CHANGCHIEN,[2] FRANK MALEY,[2] AND WILLIAM R. MONTFORT[1]

[1]Department of Biochemistry, University of Arizona, Tucson, Arizona 85721
[2]Wadsworth Center for Laboratories and Research, New York State Department of Health, Empire State Plaza, Albany, New York 12201

(RECEIVED May 13, 1997; ACCEPTED September 3, 1997)

Abstract

Thymidylate synthase (TS) is a long-standing target for anticancer drugs and is of interest for its rich mechanistic features. The enzyme catalyzes the conversion of dUMP to dTMP using the co-enzyme methylenetetrahydrofolate, and is perhaps the best studied of enzymes that catalyze carbon–carbon bond formation. Arg 126 is found in all TSs but forms only 1 of 13 hydrogen bonds to dUMP during catalysis, and just one of seven to the phosphate group alone. Despite this, when Arg 126 of TS from *Escherichia coli* was changed to glutamate (R126E), the resulting protein had k_{cat} reduced 2000-fold and K_m reduced 600-fold. The crystal structure of R126E was determined under two conditions—in the absence of bound ligand (2.4 Å resolution), and with dUMP and the antifolate CB3717 (2.2 Å resolution). The first crystals, which did not contain dUMP despite its presence in the crystallization drop, displayed Glu 126 in a position to sterically and electrostatically interfere with binding of the dUMP phosphate. The second crystals contained both dUMP and CB3717 in the active site, but Glu 126 formed three hydrogen bonds to nearby residues (two through water) and was in a position that partially overlapped with the normal phosphate binding site, resulting in a ~1 Å shift in the phosphate group. Interestingly, the protein displayed the typical ligand-induced conformational change, and the covalent bond to Cys 146 was present in one of the protein's two active sites.

Keywords: enzyme mechanism; inhibitor; mutation; X-ray crystallography

Thymidylate synthase (TS) provides the sole de novo synthetic pathway for the production of an essential DNA nucleotide, dTMP, in all cells examined. Because of this fact, TS has long been targeted for inhibition by anticancer drugs. The extensive biochemical studies in support of this endeavor have revealed a complicated enzymatic mechanism for TS that has become a paradigm for carbon transfer reactions (recently reviewed in Carreras & Santi, 1995; Hardy, 1995).

TS is perhaps the most conserved enzyme known, and all TSs appear to employ identical catalytic mechanisms and to have similar ligand-binding and inhibition profiles. TS from *E. coli* is best studied structurally and is the subject of the present report. The enzyme is a homodimer of ~61,000 Da that catalyzes the reductive methylation of dUMP to dTMP. Both carbon and hydride are transferred from the cofactor methylenetetrahydrofolate (CH_2THF) during catalysis, leading to the production of dihydrofolate (DHF). Shown in Figure 1 are the relevant intermediates in this reaction. Catalysis is initiated by nucleophilic attack of Cys 146[3] on C6 of the dUMP pyrimidine ring, leading to covalent bond formation. The reaction proceeds through an intermediate containing an additional covalent bond between dUMP and CH_2THF (intermediate III), proton abstraction from C5 of the pyrimidine ring, hydride transfer, and product release. An extensive ligand-induced conformational change accompanies catalysis (Lockshin & Danenberg, 1980; Matthews et al., 1990b; Montfort et al., 1990).

A stable analog to intermediate III can be formed with the inhibitor 5-fluoro-dUMP (FdUMP), which is the active form of anticancer drug 5-fluorouracil produced in vivo, and which has been extensively characterized crystallographically (Matthews et al.,

Reprint requests to: William R. Montfort, Department of Biochemistry, University of Arizona, Tucson, Arizona 85721; e-mail: montfort@u.arizona.edu.

Abbreviations: FdUMP, 5-fluro-dUMP; CH_2THF, methylenetetrahydrofolate; TS, thymidylate synthase; DHF, dihydrofolate; CB3717, 10-propargyl-5,8-dideazafolate; DTT, dithiothreitol.

[3]Numbering: Residue numbers for *E. coli* TS are used throughout the paper. The conversion to *L. casei* TS numbering is as follows: I + 2 for I ≤ 87, I + 52 for I > 87. Amino acids from one monomer that appear in the active site of the other monomer are indicated by a prime, as in 126′. Ordered water molecules are numbered and named according to the residue with which they are associated (e.g., Wat_2E58 is the second water bound to Glu 58).

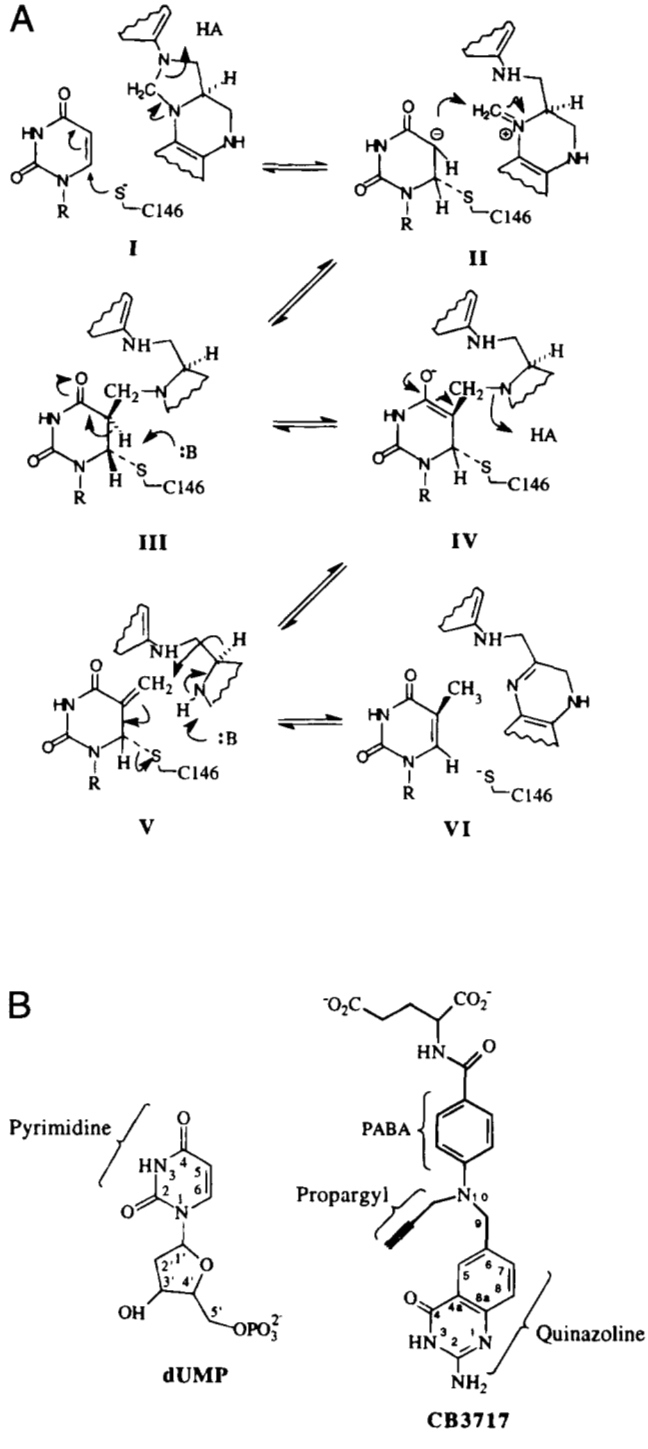

Fig. 1. (**A**) Proposed mechanism for catalysis by TS. The covalent bond between Cys 146 and dUMP is shown as a dashed line to reflect the proposed instability in the bond during catalysis (Hyatt et al., 1997). (**B**) Chemical structure and numbering for dUMP and 10-propargyl-5,8-dideazafolate (CB3717).

1990b; Hyatt et al., 1997). We have recently suggested that the poor density observed for the covalent bond between Cys 146 and nucleotide in this and other complexes may reflect a weak or polarized bond during catalysis that is required to help the enzyme avoid a deep free-energy well, and to increase the acidity of the C5 proton (Hyatt et al., 1997).

To further understand the details of TS catalysis, we are investigating the structural effects of certain mutations in the protein. The TS dimer contains two identical active sites largely composed of amino acids from a single monomer, but which contain a few residues from the second monomer in the dimer (indicated with a prime). Arg 126′ and Arg 127′ are two residues contributed from the "second" monomer into the "first" active site, and are two of four invariant arginines that contact the phosphate of dUMP during catalysis (illustrated in Fig. 2). Mutation of Arg 127′ leads to only small changes in catalytic rate (Climie et al., 1990; Michaels et al., 1990; Santi et al., 1990); however, mutation of Arg 126′ can lead to nearly inactive enzyme (Climie et al., 1990; Michaels et al., 1990; Maley et al., 1995). The latter finding was surprising because Arg 126′ makes only 1 of 13 contacts with substrate, and is unlikely to play a catalytic role beyond binding to substrate.

We determined the crystal structure of TS mutant Arg 126 → Glu (R126E) to investigate the effects of mutation on ligand-induced conformational change and covalent addition of Cys 146 to dUMP. Model building had suggested Glu 126 could simply rotate out of the active site to relieve electrostatic repulsion with the dUMP phosphate, yet the R126E mutant was ~2000-fold less active than wild-type TS. Two crystal structures of R126E were obtained: the first from crystals grown in the presence of dUMP, and the second in the presence of dUMP and CB3717, an analog of CH_2THF that displays a nanomolar inhibition constant (Jones et al., 1981; Pogolotti et al., 1986). In both proteins, Glu 126′ occupied the same position as Arg 126′ in the wild-type protein, resulting in not only electrostatic, but also steric interference with the dUMP phosphate. Interestingly, the ternary complex displayed a closed conformation and maintained a covalent bond between Cys 146 and dUMP despite the ~1 Å shift in the dUMP phosphate position.

Results

Catalysis by R126E

Both k_{cat} and K_m were severely changed in the mutant protein. k_{cat} was found to be 0.0035 s^{-1} for R126E, ~2000-fold less than that for the wild-type protein, and K_m for dUMP found to be 3.0 mM, ~600-fold higher than that for the wild-type protein (Maley & Maley, 1988).[4] Thus, the kinetic data suggest both substrate binding and active site arrangement were potentially modified in the mutant protein.

Crystal structure determinations

The R126E mutant was crystallized under two conditions. First, the protein was crystallized with dUMP and the antifolate CB3717 (Fig. 1), a complex that, for the wild-type protein, results in a ligand arrangement similar to that for substrates (Finer-Moore et al., 1990; Matthews et al., 1990a, 1990b; Montfort et al., 1990; Hyatt et al., 1997). These crystals were isomorphous with the wild-type protein crystallized under similar conditions (Montfort

[4] K_m for the wild-type protein was mistakenly listed as 5×10^{-5} M in (Maley & Maley, 1988). The correct value is 5×10^{-6} M.

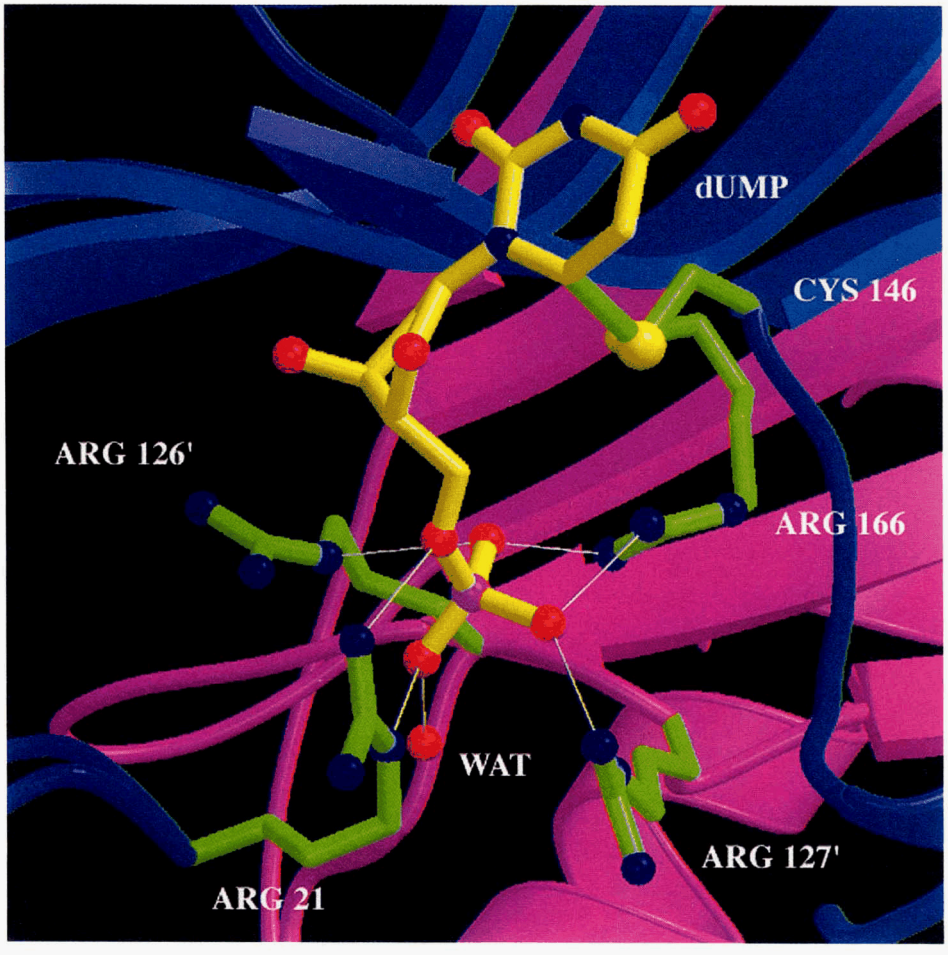

Fig. 2. Ribbon drawing of the wild-type ternary complex with dUMP and CB3717, showing all four active site arginines. Monomer one is shown in blue, and monomer two in pink. Side-chain covalent bonds and the covalent bond to dUMP are shown in green, nitrogens in blue, oxygens in red, and sulfur in yellow. dUMP is shown in yellow, and CB3717 has been left out for clarity. Hydrogen bonds to the phosphate oxygens are indicated with white lines. Arg 126′ and Arg 127′ are from the second monomer. This figure was produced with the programs MOLSCRIPT (Kraulis, 1991) and Raster 3D (Bacon & Anderson, 1988; Merritt & Murphy, 1994)

et al., 1990), diffracted to 2.2 Å nominal resolution, and were found to contain both ligands in the active site. Second, the protein was crystallized with dUMP alone under conditions that result in a binary complex with the wild-type protein (Roberts & Montfort, in prep). These crystals were isomorphous with the wild-type crystals, diffracted to 2.4 Å nominal resolution, but did not contain ligand in the active site. Conventional model building and crystallographic refinement were sufficient to determine the structures of the two complexes. The final crystallographic results are shown in Table 1.

R126E–dUMP–CB3717 ternary complex

The overall topology of the R126E ternary complex is similar to that of the wild-type protein, and displays the closed TS conformation. Likewise, the position of the inhibitor is essentially unchanged. Glu 126′ is coincident with the position of Arg 126′ in the wild-type protein, and is well ordered in both active sites (Fig. 3). This position places the Glu 126′ side chain such that the carboxylate group overlaps with the position for dUMP in the wild-type structure, resulting in a ~1 Å shift of the dUMP phosphate toward Arg 127′, which is dislodged from the active site and as a result becomes poorly ordered in the mutant structure. Had the dUMP phosphate not shifted, the distance between it and the carboxylate of dUMP Glu 126′ would have been ~2.2 Å.

The asymmetric unit (unique portion) of the ternary complex crystal form contains the full TS dimer, and so the two halves of the dimer are not constrained to be identical. In the first active site, dUMP is well ordered except for those atoms that shift due to the position of Glu 126′ (ribose atoms C4′ and C5′, and the phosphate). The pyrimidine ring is in the same position as in the wild-type structure and covalently linked to Cys 146 (Fig. 3A). This bond refined to a distance of 2.0 Å. In the second active site, the density for the dUMP is somewhat worse, however, especially for the covalent bond (Fig. 3B). Refinement of the structure with the C6–Cys 146 covalent bond restrained to 2.0 Å resulted in a bond length of 2.4 Å. Modeling the dUMP without a covalent bond and the pyrimidine ring as planar resulted in a C6–sulfur distance of 2.7 Å, about half way between the van der Waals and covalent distances for carbon and sulfur atoms. The most likely explanation

Table 1. *Crystallographic results*

Complex	dUMP–CB3717	dUMP
Space group	$P6_3$	$I2_13$
Cell constants (Å)	a = 126.61	a = 132.7
	c = 67.30	
Resolution (Å)	2.2	2.4
Unique reflections	33,337	14,066
Total reflections	121,313	88,083
Completeness (%)		
(overall/outer shell)	90/87	92/77
R_{sym}[a]	5.3	10.1
Multiplicity	3.6	6.2
R_{cryst}[b]	16.6	18.5
R_{free}[c]	19.4	22.5
RMS Deviations		
Bond distances (Å)	0.011	0.011
Bond angles (deg.)	1.5	1.5
No. of water molecules	190	48
PDB accession number	1aiq	1ajm

[a] $R_{sym} = 100(\Sigma_h|I_h - I|)/(\Sigma_h I_h)$, where I is the mean intensity of all symmetry related reflections I_h.

[b] $R_{cryst} = 100(\Sigma||F_{obs} - F_{calc}|)/(\Sigma F_{obs})$, for all non-zero reflections.

[c] R_{free} as for R_{cryst} using a subset of the data (5%) not included in the refinement, as implemented in X-PLOR (Brunger, 1992).

for this is that the stability of the covalent adduct has been reduced in the mutant protein, leading to a mixed population of covalently linked and unlinked dUMP molecules in the second monomers in the crystal (discussed further below). This state is apparently accommodated by the crystalline environment of the second monomer, but not the first, and must be due to subtle differences between the two monomers, since, aside from the covalent adduct, the two active sites are nearly identical.

A series of new hydrogen bonds stabilize the Glu 126′ position (Fig. 4). The hydrogen bond between Arg 126′ and the dUMP phosphate in the wild-type structure is replaced by a hydrogen bond to the Glu 126′ carboxylate (2.5 Å; all distances quoted for the ternary complex are the average of both active sites unless otherwise noted). This same Glu 126′ oxygen also hydrogen bonds to Ser 167 (2.7 Å). The other carboxylate oxygen hydrogen bonds to two new active site water molecules, Wat_1E126′ (2.9 Å) and Wat_2E126′ (3.2 Å). These water molecules are well anchored, forming additional hydrogen bonds to Tyr 209 (2.6 Å), Asp 20 (2.9 Å), Thr 26 (2.9 Å), and probably Asp 205 (3.2 Å), although this bond is less certain. Thus, the mutated residue Glu 126′ is firmly tied in place, and well positioned to interfere with dUMP binding.

Arg 21 and Arg 166 track the dUMP phosphate to its new position and maintain three of the four hydrogen bonds to dUMP found in the wild-type complex (Fig. 4; 2.8 Å and 2.5 Å for Arg 166, 2.7 Å for Arg 21). The fourth hydrogen bond (to Arg 21) appears not to be present in either active site, although the residue is somewhat disordered and its position, therefore, uncertain, especially in the second active site. In contrast, Arg 127′ flips out of the active sites of both monomers and becomes poorly ordered in the crystal. The relative positioning of dUMP and nearby amino acids for the wild-type and mutant structures is shown in Figure 5, after superpositioning of the two structures.

Unliganded structure

To assess whether Glu 126′ retains the extensive series of hydrogen bonds stabilizing its position in the ternary complex—and, thus, in a position to sterically interfere with initial dUMP binding—R126E was crystallized in the presence of dUMP alone. Under these conditions, a different crystal form is obtained that has only a monomer in the asymmetric unit (the second monomer of the dimer is related to the first through a crystallographic twofold symmetry axis). The resulting structure revealed the protein to be in the open TS conformation, as found for the wild-type protein, but without dUMP present in the active site (Fig. 6). Glu 126′ was again coincident with the position for Arg 126′ in the wild-type protein, but was somewhat less well ordered. The hydrogen bond to Ser 167 found in the ternary complex is also found in the unliganded structure (2.3 Å), but the two water molecules linking Glu 126′ to Asp 20, Thr 26, Asp 205, and Tyr 209 are both missing. In the open conformation, these residues are too far from Glu 126′ for a single water molecule to bridge the gap between them (e.g., the distance between hydrogen bonding groups on Glu 126′ and those on Thr 26 and Tyr 209 increase by 1.9 and 1.4 Å, respectively). Both Arg 21 and Arg 127′ are poorly ordered in the absence of dUMP, and Arg 127′ once again lies out of the active site.

There is a small amount of electron density in the mutant structure occupying the position for dUMP in the wild-type structure (Fig. 6). We have interpreted this as three water molecules, but it is possible that a small percentage of active sites in the crystal contain dUMP.

Discussion

We have determined two crystal structures of the marginally active TS mutant R126E: one bound to dUMP and CB3717, and the other without bound ligand despite the presence of 1.5 mM dUMP in the crystallizing drop. Several reasons for the severe drop in catalytic activity are suggested by these structures. In the ternary complex, Glu 126′ is anchored by three hydrogen bonds into a position that overlaps with the dUMP phosphate binding pocket, thus sterically interfering with substrate binding (Fig. 4). Binding may also be reduced through electrostatic repulsion between Glu 126′ and the dUMP phosphate, as both groups should be negatively charged at neutral pH, at least before complex formation. That this is at most only a minor effect is suggested by the Arg 126′ → Gln mutant (R126Q′), which is only about sixfold more active than R126E′ (Maley, unpub. obs.). Glutamine is isosteric with glutamate, and should be able to form similar hydrogen bonds to those that stabilize the glutamate position in the R126E′–dUMP–CB3717 structure. It is interesting that Glu 126′ is completely buried in the ternary complex, with all possible hydrogen bonds satisfied. It is likely that the group is uncharged (fully protonated) in this arrangement, and therefore most likely displays an altered pK_a in the ternary complex.

The dUMP pyrimidine ring placement is nearly identical to that of the wild-type structure and covalently linked to Cys 146 in one active site, despite the ~1 Å shift in the dUMP phosphate position. The position of the pyrimidine ring is influenced through six hydrogen bonds, four to the pyrimidine ring and two to the ribose (Fig. 4), and by extensive van der Waals contacts with the quinazoline and propargyl groups of CB3717, which binds identically to both wild-type and mutant proteins (not shown). That these interactions are sufficiently strong to overcome repulsion between

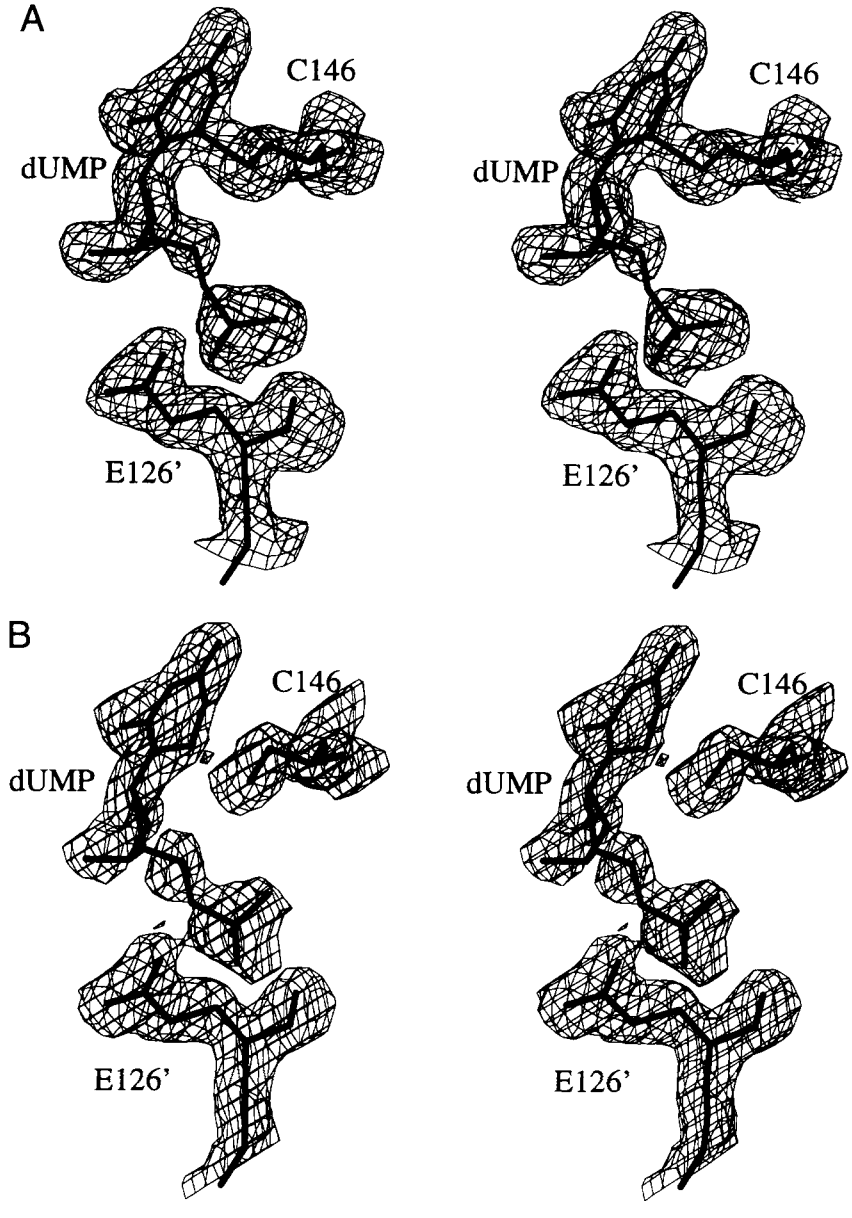

Fig. 3. Electron density for the R126E–dUMP–CB3717 ternary complex. (**A**) Shown is the final 2Fo-Fc electron density map for the mutated residue (Glu 126′), substrate, and Cys 146 in the first active site, at a contour level of 1 σ. Electron density for Glu 126′ and the covalent bond between dUMP and Cys 146 are clearly displayed, but electron density for ribose atoms C4′ and C5′, as well as the phosphate group, is much worse. (**B**) Second active site, contoured as in (A). The density for dUMP is worse and dUMP appears to be mostly without covalent linkage to Cys 146 (see text). This figure and Fig. 6 drawn with O (Jones et al., 1991).

Glu 126′ and the dUMP phosphate, as well as to induce the closed protein conformation, points to the usefulness of quinazoline-based TS inhibitors. Indeed, CB3717 has a nanomolar inhibitory constant and an extremely long association half-life (Pogolotti et al., 1986). However, the loss of covalent bond formation in one active site suggests the mutant protein is less able to achieve covalent intermediate III (Fig. 1), which probably accounts in part for the observed reduction in k_{cat}.

Thus, a picture emerges for why the R126E mutant is such a poor enzyme. The 600-fold increase in K_m is almost certainly due to reduced binding of substrate. The 2000-fold reduction in k_{cat} appears to be due to a reduced ability to reach intermediate III, suggesting that formation of this intermediate is rate limiting in the mutant. Apparently, very slight changes in the active site geometry can lead to reduced stability in the thiol adduct to dUMP (see below). It is also possible that the rate for the ligand-induced conformational change, which must occur for formation of intermediate III, has been reduced in the mutant, further reducing k_{cat}.

We have recently suggested that the TS covalent intermediate may be unstable during catalysis, based on variable density for the covalent bond in a variety of complexes (Hyatt et al., 1997). The present work supports this contention in that the two active sites of the ternary complex are nearly identical (the rms deviation in Cα positions is 0.31 Å) and yet display differences in the formation of

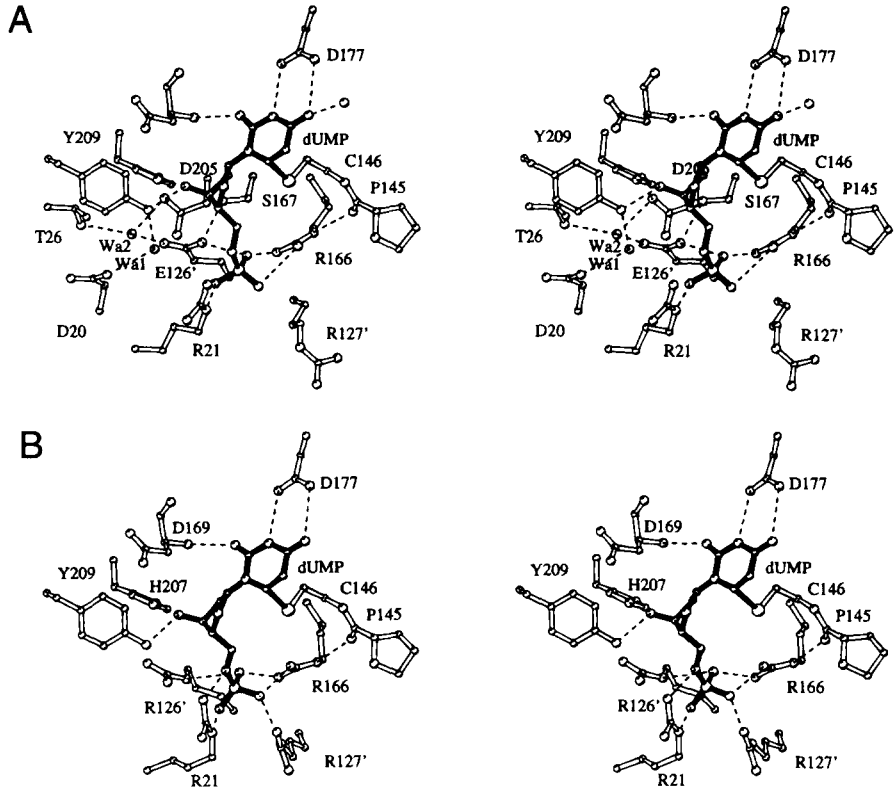

Fig. 4. (**A**) Hydrogen bonds between dUMP and specific amino acids in the ternary complex R126E–dUMP–CB3717. dUMP is shown with filled bonds, protein with open bonds, hydrogen bonds as dashed lines, and water molecules as spheres. Carbon atoms are indicated with smaller spheres than oxygen, nitrogen, sulfur, and phosphate atoms. The two water molecules Wat_1E126' and Wat_2E126' are labeled as Wa1 and Wa2, respectively. (**B**) Wild-type protein in the same complex (Montfort et al., 1990). This figure and Figure 5 drawn with MOLSCRIPT (Kraulis, 1991).

the covalent bond with Cys 146. An alternative explanation for the difference between the two active sites is that the mutation has unmasked the apparent half-the-sites reactivity of the TS dimer (Maley et al., 1995) even at the high ligand concentrations used in crystallization, as has recently been suggested to explain active site differences observed in the structure of the E58Q TS mutant (Sage et al., 1996). This explanation seems less likely to us for the present work as the wild-type TS–dUMP–CB3717 ternary complex exists without a covalent link to Cys 146 in crystal forms other than those used here (Roberts & Montfort, in prep.).

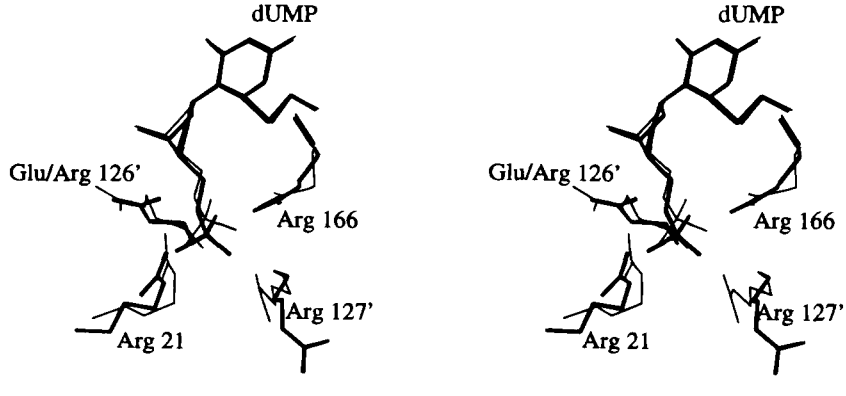

Fig. 5. Superimposed structures of TS.dUMP.PDDF (thin lines) and R126E–dUMP–CB3717 (thick lines).

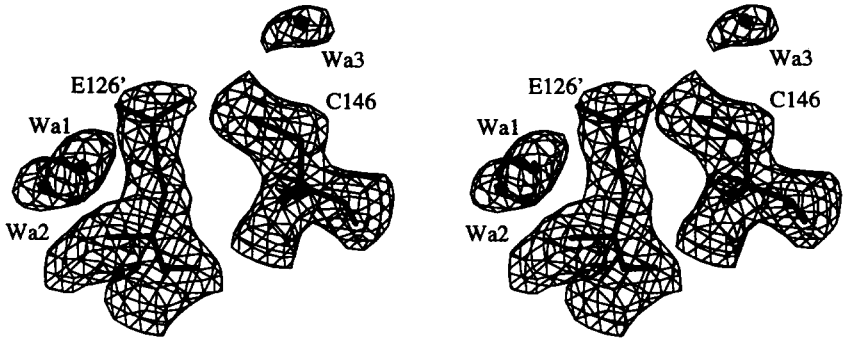

Fig. 6. Electron density for R126E crystals grown in the presence of dUMP. Shown is the final 2Fo-Fc electron density map for the mutated residue (Glu 126′), Cys 146, and three water molecules in the region where dUMP binds in the wild-type structure, at a contour level of 1 σ. Electron density for the Glu 126′ side chain is somewhat worse than that for the main chain atoms.

Methods

Enzyme preparation and characterization

The R126E mutant *E. coli* thymidylate synthase protein was prepared from an overexpressing strain of *E. coli* as previously described (Maley et al., 1995). Enzyme activity was measured using the spectrophotometric assay of (Wahba & Friedkin, 1962) with modification (Maley et al., 1995).

X-ray crystallography

For crystal growth, the enzyme was dialyzed against 20 mM potassium phosphate, pH 7.0, 0.1 M EDTA, and 10 mM dithiothreitol (DTT). Cubic crystals of the binary complex were grown at room temperature using the hanging drop method and conditions similar to those previously published (Perry et al., 1990) except that DTT was substituted for 2-mercaptoethanol. A solution of R126E TS (12 mg/mL), 3 mM dUMP, 20 mM potassium phosphate (pH 8.0), and 4 mM DTT was mixed 1:1 with precipitant solution (2.5 M ammonium sulfate, 20 mM potassium phosphate, pH 8.0, and 4 mM DTT) and equilibrated against the precipitant solution. The resulting crystals (0.32 × 0.32 × 0.20 mm) belonged to space group $I2_13$ and were isomorphous with those of the wild-type protein.

Hexagonal crystals of the ternary complex were also grown at room temperature using the hanging drop method and conditions similar to those previously published (Montfort et al., 1990; Fauman et al., 1994). A solution of R126E TS (10 mg/mL), 3 mM dUMP, 3 mM CB3717, 20 mM potassium phosphate (pH 7.5), and 4 mM DTT was mixed 1:1 with precipitant solution (2.5 M ammonium sulfate, 20 mM potassium phosphate, pH 7.5, and 4 mM DTT) and equilibrated against the precipitant solution. The resulting crystals (0.6 × 0.4 × 0.6 mm) belonged to space group $P6_3$ and were isomorphous with those of the wild-type protein.

A single crystal was used to obtain diffraction data for each complex on an Enraf Nonius diffractometer equipped with a FAST area detector attached to a Cu anode X-ray source. Data reduction was performed with software packages MADNES (Messerschmidt & Pflugrath, 1987), PROCOR (Kabsch, 1988), and FBSCALE (Weissman, 1982). Electron density maps were calculated using CCP4 (Collaborative Computational Project, 1994). Both crystal forms were isomorphous with crystals of the wild-type protein prepared under similar conditions. The structures of TS–dUMP–CB3717 and TS–dUMP were used as a starting models for refinement with programs X-PLOR (Brunger, 1988, 1993) and TNT (Tronrud et al., 1987), with local rebuilding using O (Jones et al., 1991). Final statistics for data collection and model refinement are shown in Table 1.

Acknowledgments

We thank Drs. Sue Roberts and Andrzej Weichsel for technical assistance. This work was supported in part by American Cancer Society grant DHP-45 (W.R.M.) and National Cancer Institute Grant CA44355, USPHS/HHS (F.M.).

References

Bacon DJ, Anderson WF. 1988. A fast algorithm for rendering space-filling molecule pictures. *J Mol Graphics 6*:219–220.

Brunger AT. 1988. Crystallographic refinement by simulated annealing. Application to a 2.8 Å resolution structure of aspartate aminotransferase. *J Mol Biol 203*:803–816.

Brunger AT. 1992. Free *R* value: A novel statistical quantity for assessing the accuracy of crystal structures. *Nature 355*:472–475.

Brunger AT. 1993. *X-PLOR: A system for X-ray crystallography and NMR*. New Haven, Connecticut: Yale University Press.

Carreras CW, Santi DV. 1995. The catalytic mechanism and structure of thymidylate synthase. *Annu Rev Biochem 64*:721–762.

Climie S, Ruiz-Perez L, Gonzalez-Pacanowska D, Prapunwattana P, Cho S-W, Stroud R, Santi DV. 1990. Saturation site-directed mutagenesis of thymidylate synthase. *J Biol Chem 265*:18776–18779.

Collaborative Computational Project N. 1994. The CCP4 suite: Programs for protein crystallography. *Acta Crystallogr D50*:760–763.

Fauman EB, Rutenber EE, Maley GF, Maley F, Stroud RM. 1994. Water-mediated substrate/product discrimination: The product complex of thymidylate synthase at 1.83 Å. *Biochemistry 33*:1502–1511.

Finer-Moore JS, Montfort WR, Stroud RM. 1990. Pairwise specificity and sequential binding in enzyme catalysis: Thymidylate synthase. *Biochemistry 29*:6977–6986.

Hardy LW. 1995. Structural aspects of the inhibition and catalytic mechanism of thymidylate synthase. *Acta Biochim Polon 42*:367–380.

Hyatt DC, Maley F, Montfort WR. 1997. Use of strain in a stereospecific catalytic mechanism: Crystal structures of *Escherichia coli* thymidylate synthase bound to FdUMP and methylenetetrahydrofolate. *Biochemistry 36*:4585–4594.

Jones TA, Zou JY, Cowan SW, Kjelgard M. 1991. Improved methods for building protein models in electron density maps and the location of errors in these models. *Acta Crystallogr A47*:110–119.

Jones TR, Calvert AH, Jackman AL, Brown SJ, Jones M, Harrap KR. 1981. A potent antitumor quinazoline inhibitor of thymidylate synthetase: Synthesis, biological properties, and therapeutic results in mice. *Eur J Cancer 17*:11–19.

Kabsch W. 1988. Evaluation of single-crystal X-ray diffraction data from a position-sensitive detector. *J Appl Crystallogr 21*:916–934.

Kraulis PJ. 1991. MOLSCRIPT: A program to produce both detailed and schematic plots of protein structures. *J Appl Crystallogr 24*:946–950.

Lockshin A, Danenberg PV. 1980. Hydrodynamic behavior of human and bacterial thymidylate synthetases and thymidylate synthetase-5-fluoro-2′deoxyuridylate-5,10-methylenetetrahydrofolate complexes. Evidence for large conformational changes during catalysis. *Biochemistry 19*:4244–4251.

Maley F, Pedersen-Lane J, Changchien L. 1995. Complete restoration of activity to inactive mutants of *Escherichia coli* thymidylate synthase: Evidence that *E. coli* thymidylate synthase is a half-the-sites activity enzyme. *Biochemistry 34*:1469–1474.

Maley GF, Maley F. 1988. Properties of a defined mutant of *Escherichia coli* thymidylate synthase. *J Biol Chem 263*:7620–7627.

Matthews DA, Appelt K, Oatley SJ, Xuong NH. 1990a. Crystal structure of *Escherichia coli* thymidylate synthase containing bound 5-fluoro-2′-deoxyuridylate and 10-propargyl-5,8-dideazafolate. *J Mol Biol 214*:923–936.

Matthews DA, Villafranca JE, Janson CA, Smith WW, Welsh K, Freer S. 1990b. Stereochemical mechanism of action for thymidylate synthase based on the X-ray structure of the covalent inhibitor ternary complex with 5-fluoro-2′-deoxyuridylate and 5,10-methylenetetrahydrofolate. *J Mol Biol 214*:937–948.

Merritt EA, Murphy MEP. 1994. Raster3D version 2.0—A program for photorealistic molecular graphics. *Acta Crystallogr D50*:869–873.

Messerschmidt A, Pflugrath JW. 1987. Crystal orientation and X-ray pattern prediction routines for area-detector diffractometer systems in macromolecular crystallography. *J Appl Crystallogr 20*:306–315.

Michaels ML, Kim CW, Matthews DA, Miller JH. 1990. *Escherichia coli* thymidylate synthase: Amino acid substitutions by suppression of amber nonsense mutations. *Proc Natl Acad Sci USA 87*:3957–3961.

Montfort WR, Perry KM, Fauman EB, Finer-Moore JS, Maley GF, Hardy L, Maley F, Stroud RM. 1990. Structure, multiple site binding, and segmental accommodation in thymidylate synthase on binding dUMP and an antifolate. *Biochemistry 29*:6964–6977.

Perry KM, Fauman EB, Finer-Moore JS, Montfort WR, Maley GF, Maley F, Stroud RM. 1990. Plastic adaptation toward mutations in proteins: Structural comparison of thymidylate synthases. *Proteins Struct, Funct, Genet 8*:315–333.

Pogolotti AL Jr, Danenberg PV, Santi DV. 1986. Kinetics and mechanism of interaction of 10-propargyl-5,8-dideazafolate with thymidylate synthase. *J Med Chem 29*:478–482.

Sage CR, Rutenber EE, Stout TJ, Stroud RM. 1996. An essential role for water in an enzyme reaction mechanism: The crystal structure of the thymidylate synthase mutant E58Q. *Biochemistry 35*:16270–16281.

Santi DV, Pinter K, Kealey J, Davisson VJ. 1990. Site-directed mutagenesis of arginine 179 of thymidylate synthase. A nonessential substrate-binding residue. *J Biol Chem 265*:6770–6775.

Tronrud DE, Ten Eyck LF, Matthews BW. 1987. General purpose least-squares refinement program for macromolecular structures. *Acta Crystallogr A43*:489–501.

Wahba AJ, Friedkin M. 1962. Direct spectrophotometric evidence for oxidation of tetrahydrofolate during enzymatic synthesis of thymidylate. *J Biol Chem 237*:3794–3801.

Weissman L. 1982. Strategies for extracting isomorphous and anomalous signals. In: Sayre, D., ed. *Computational crystallography*. Oxford: Clarendon Press. pp 56–63.